Net Baryon Density in Au + Au Collisions at the Relativistic Heavy Ion Collider

Steffen A. Bass,[1,2] Berndt Müller,[1] and Dinesh K. Srivastava[3,4]

[1]*Department of Physics, Duke University, Durham, North Carolina 27708-0305, USA*
[2]*RIKEN BNL Research Center, Brookhaven National Laboratory, Upton, New York 11973, USA*
[3]*Variable Energy Cyclotron Centre, 1/AF Bidhan Nagar, Kolkata 700 064, India*
[4]*Physics Department, McGill University, 3600 University Street, Montreal, H3A 2T8, Canada*

(Received 29 December 2002; revised manuscript received 24 April 2003; published 1 August 2003)

We calculate the net-baryon rapidity distribution in Au + Au collisions at the Relativistic Heavy Ion Collider (RHIC) in the framework of the parton cascade model (PCM). Parton rescattering and fragmentation leads to a substantial increase in the net-baryon density at midrapidity over the density produced by initial primary parton-parton scatterings. The PCM is able to describe the measured net-baryon density at RHIC.

DOI: 10.1103/PhysRevLett.91.052302 PACS numbers: 25.75.–q, 12.38.Mh

First experiments at the Relativistic Heavy Ion Collider (RHIC) have shown that the matter created in the central rapidity region contains a significant excess of baryons over antibaryons. While a slight baryon excess was not unexpected, the magnitude of the net-baryon multiplicity density $dN_{\mathrm{B}-\overline{\mathrm{B}}}/dy \approx 19 \pm 2$ [1,2] at $\sqrt{s_{NN}} = 130$ GeV and $\approx 14 \pm 4$ [3] at $\sqrt{s_{NN}} = 200$ GeV is higher than what many theoretical models had predicted [4]. In particular, models in which the deposition of energy at midrapidity is driven by quasiclassical glue fields [5] or fragmenting color flux tubes [6], which produce quarks and antiquarks in equal abundance, underpredicted the data. On the other hand, models invoking baryon junctions [7,8] for the transport of baryon number from the beam rapidity into the central region $y \approx 0$ have done remarkably well. The baryon junction mechanism was originally proposed as a means to understand baryon-number annihilation and stopping in elementary $p + p$ and $p + \bar{p}$ reactions [9]. In this Letter we shall address the question of whether only baryon junctions provide a mechanism capable of explaining the RHIC data, or whether they can also be understood in the framework of a more conventional picture, based on parton distributions and perturbative quantum chromodynamics (pQCD) driven multiple interactions.

Two effects based on established physics can contribute to the baryon excess at midrapidity. First, the measured parton-distribution functions in the nucleon are well known to exhibit a substantial asymmetry between quark and antiquark distributions at moderately small values of Bjorken-x ($x \approx 0.01$) relevant for RHIC energies (Fig. 1, see below). Second, it is known from experiments with $p + A$ collisions that multiple scattering is quite effective in transporting baryons to smaller rapidities [11]. The parton cascade model (PCM) [12–14] provides a natural framework for exploring the consequences of these two effects quantitatively.

Devised as a description of the early, preequilibrium phase of a nucleus-nucleus collision at relativistic energy, the PCM does not include a description of hadronization and the subsequent scattering among hadrons. These late-stage processes, however, are not expected to alter the distribution of net-baryon number with respect to rapidity, because baryon diffusion in a hadronic gas is slow [15] and the net-baryon number is locally conserved. We therefore believe that these limitations of the PCM approach should not stand in the way of an adequate explanation of the net-baryon distribution. In this Letter, we present calculations of the net-baryon multiplicity density distribution in Au + Au collisions at 130 and 200 GeV center-of-mass energy per nucleon pair.

The fundamental assumption underlying the PCM is that the state of the dense partonic system can be characterized by a set of one-body distribution functions $F_i(x^\mu, p^\alpha)$, where i denotes the flavor index ($i = g, u, \bar{u}, d, \bar{d}, \ldots$) and x^μ, p^α are coordinates in the eight-dimensional phase space. The partons are assumed to be on their mass shell, except before the first scattering. In

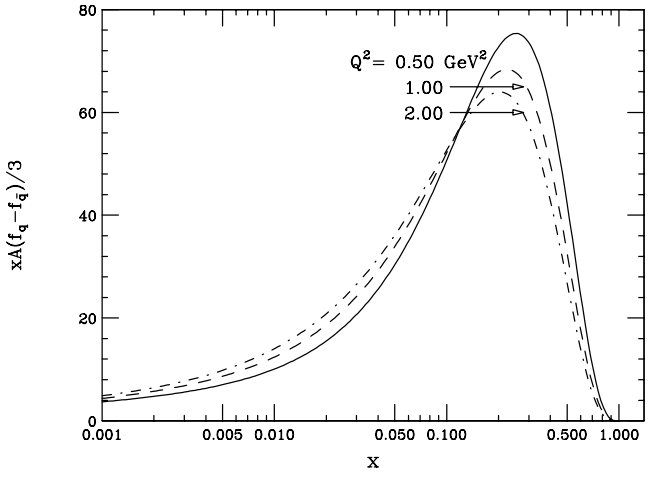

FIG. 1. Net baryon content of the partonic distribution function of gold-nucleus at the factorization scales (Q_0^2) of 0.50 GeV^2 (solid curve), 1.00 GeV^2 (dashed curve), and 2.00 GeV^2 (dot-dashed curve), for the GRV-HO [10] parametrization. Parton shadowing is not included.

our numerical implementation, the GRV-HO parametrization [10] is used, and the parton-distribution functions are sampled at an initialization scale Q_0^2 to create a discrete set of particles. Partons generally propagate on shell and along straightline trajectories between interactions. Before their first collision, partons may have a spacelike four-momentum, especially if they are assigned an "intrinsic" transverse momentum.

The time evolution of the parton distribution is governed by a relativistic Boltzmann equation:

$$p^\mu \frac{\partial}{\partial x^\mu} F_i(x, \vec{p}) = C_i[F], \tag{1}$$

where the collision term C_i is a nonlinear functional of the phase-space distribution function. The calculations discussed below include all lowest-order QCD scattering processes between massless quarks and gluons [16]. A low momentum-transfer cutoff $p_T^{\min}$ is needed to regularize the infrared divergence of the perturbative parton-parton cross sections. Additionally, we include the branchings $q \to qg$, $q \to q\gamma$, $g \to gg$, and $g \to q\bar{q}$ [17]. The soft and collinear singularities in the showers are avoided by terminating the branchings when the virtuality of the timelike partons drops below $\mu_0 = 1$ GeV. Some of these aspects were originally discussed in [13]. The present Letter is based on our thoroughly revised, corrected, and extensively tested implementation of the parton cascade model, named VNI/BMS [14].

Figure 1 shows the net baryon-number distribution $xA[f_q(x) - f_{\bar{q}}(x)]/3$ with the Bjorken-x variable. We have defined,

$$xf_q(x) = \sum_{i=u,d,s} xF_i(x), \tag{2}$$

where $F_i(x)$ is the isospin averaged parton-distribution function for a nucleon in the gold nucleus, so that

$$F_i(x) = \frac{Z}{A} F_i^P(x) + \frac{(A-Z)}{A} F_i^N(x), \tag{3}$$

where the superscripts P and N stand for protons and neutrons. Thus the figure brings out the asymmetry between the quark and antiquark distributions at moderately small values of Bjorken-x ($x \approx 0.01$) relevant for energy deposition at midrapidity at RHIC energies. The various lines denote different initialization scales for the parton-distribution functions. This provides the basis for the evaluation of the dynamical evolution of the stopping through parton collisions, sometimes accompanied by gluon radiation and quark pair creation.

The partons in a fast moving nucleon or a nucleus are distributed both in the transverse and longitudinal directions. Because of the large longitudinal Lorentz contraction, the longitudinal momentum $p_z = xP$ is the most interesting variable. Before or immediately after the first collision of a parton, one can relate p_z to the rapidity variable $y = Y + \ln x + \ln(M/Q_s)$, where Y is the rapidity of the fast moving nucleon, M is the nucleon mass, and Q_s denotes the typical transverse momentum scale. Depending on the picture of the initial state, Q_s is either given by the average intrinsic virtuality, often called the saturation scale [18], or by the typical transverse momentum given to the parton in the first interaction which brings it onto the mass shell. In any case, $|\ln(M/Q_s)| < 1/2$ for Au + Au collisions at RHIC.

If the partons in the two gold nuclei were to decohere completely upon passing through each other without any further interaction, the resulting net-baryon rapidity distribution would be approximately given by Fig. 1—predicting a contribution to the net-baryon density of about 7 at midrapidity (with $Y = 5.4$ for $\sqrt{s_{NN}} = 200$ GeV) due to each nucleus. This is seen as follows. The baryon number in the nucleus A is given by

$$A = \frac{1}{3} A \int [x f_q(x) - x f_{\bar{q}}(x)]\, d\ln x, \tag{4}$$

so that the net baryon-distribution "contained" in the nucleus is

$$\left(\frac{dN}{dy}\right)_{B-\bar{B}} = \frac{1}{3} x A [f_q(x) - f_{\bar{q}}(x)]. \tag{5}$$

We shall see that the parton-interactions incorporated in the PCM remain consistent with this intuitive picture.

A crucial parameter of the PCM is the low momentum-transfer cutoff $p_T^{\min}$. Under certain assumptions this parameter can be determined from experimental data for elementary hadron-hadron collisions [19–21]. In the environment of a heavy-ion collision, color screening will destroy the association of partons to particular hadrons, since the density of free color charges is so high that the color screening length becomes smaller than the typical hadronic scale. In a previous publication [14] we have established a consistency limit for the allowed range of $p_T^{\min}$ by calculating the screening mass μ_D in the produced parton matter as a function of the cutoff $p_T^{\min}$ and demanding ($p_T^{\min} \geq \mu_D$). The initialization scale and low momentum cutoff of the pQCD cross sections were chosen as $Q_0^2 = (p_T^{\min})^2 = 0.50$ GeV^2 for $\sqrt{s_{NN}} = 130$ GeV and 0.59 GeV^2 for $\sqrt{s_{NN}} = 200$ GeV, respectively. The energy scaling of this parameter agrees with that determined by Eskola *et al.* [22] for the geometric minijet saturation model.

Figure 2 shows the PCM predictions for the net-baryon rapidity distributions for $\sqrt{s_{NN}} = 130$ GeV (upper panel) and 200 GeV (lower panel), respectively. The initial projectile and target rapidities are ± 4.9 for $\sqrt{s_{NN}} = 130$ GeV and ± 5.4 for $\sqrt{s_{NN}} = 200$ GeV. The calculations are done without assigning any intrinsic k_T to the partons—initially all partons move with the velocity $\beta = \pm P_z^{\mathrm{A}}/E_A$ of the nucleus in the center-of-mass frame, where P_z is the momentum and E_A is the energy of the nucleus.

Crosses in Fig. 2 denote a calculation in which the PCM has been restricted to primary-primary parton

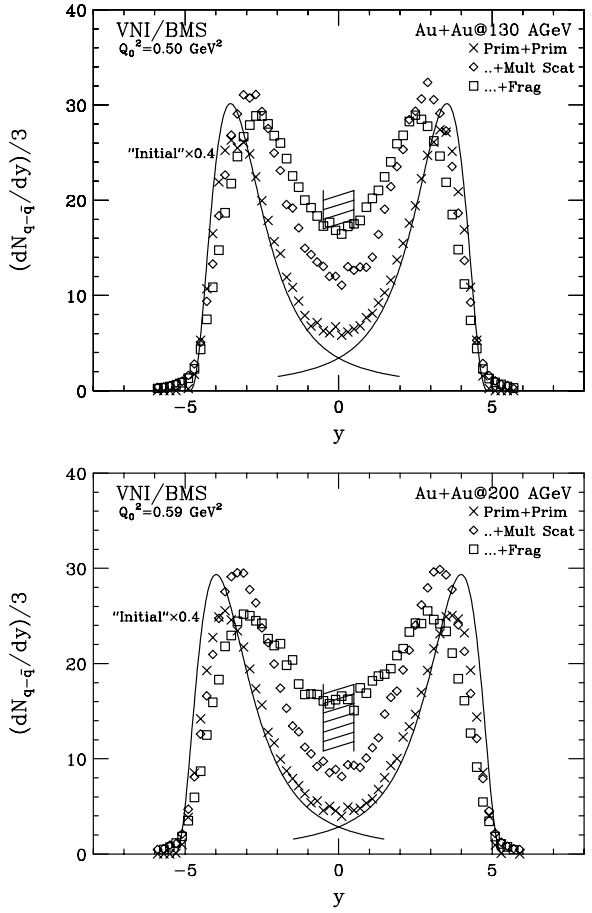

FIG. 2. Net baryon rapidity distributions for Au + Au reactions at $\sqrt{s_{NN}} = 130$ GeV (top) and $\sqrt{s_{NN}} = 200$ GeV bottom. Crosses denote a calculation in which the PCM has been restricted to primary parton scatterings, diamonds include parton rescattering, and squares include rescattering and parton fragmentation. The solid lines show the net baryon content of the partonic distribution functions for gold nuclei, scaled by an average liberation factor of 0.4 . The band at y_{CM} shows the range of experimental estimates for the net-baryon density by STAR, BRAHMS, and PHENIX.

scatterings, and therefore reflects a calculation in which each parton is allowed to scatter only once. Already one hard collision is sufficient to deposit a net surplus of quarks into the midrapidity region, resulting in a net-baryon density at $y_{cm} = 0$ of 6.3 for 130 GeV and 5.0 at 200 GeV. For comparison, the net-baryon number distribution for each colliding nucleus, scaled by a factor 0.4 from the distribution shown in Fig. 1, is shown as a solid line. The remarkable agreement demonstrates that the net-baryon number distribution produced by first parton-parton collisions is predetermined by the initial parton structure of the nuclei. The factor 0.4 is the average "liberation factor" c for partons in the PCM for the selected parameters. This factor is consistent with predictions by some gluon saturation models [23].

The diamonds in Fig. 2 represent a calculation with full parton-parton rescattering. Allowing for multiple parton collisions increases the net-baryon density at midrapidity roughly by a factor of 2 at 130 GeV and by 75% at 200 GeV, filling up the dip around midrapidity. This trend continues when parton fragmentation is included (squares): at 130 GeV fragmentation processes add another 50% to the net-baryon density at midrapidity, bringing it up to about 18, whereas at 200 GeV the net-baryon density increases to near 14. The rapidity change of a quark in each subsequent collision after its liberation in the first hard scattering yields an average rapidity shift of roughly 0.65 units per collision.

The band around midrapidity in Fig. 2 denotes the range of experimental estimates for the net-baryon density at midrapidity for 130 and 200 GeV, respectively [1–3]. These estimates depend on how the extrapolations from $(p - \bar{p})$ and $(\Lambda - \bar{\Lambda})$ to $(B - \bar{B})$ have been carried out, the extreme scenarios being the assumption of full isospin equilibration for baryons, $(B - \bar{B}) = 2(p - \bar{p})$, vs the full inclusion of the isospin asymmetry of the initial state, $(B - \bar{B}) = A/Z(p - \bar{p})$. Note that our calculation does not suffer from this uncertainty.

Figure 3 shows the net-baryon density at midrapidity as a function of the momentum cutoff $p_T^{\min}$ for Au + Au collisions at $\sqrt{s_{NN}} = 200$ GeV. Again, crosses denote the calculation restricted to primary-primary collisions, diamonds represent the full rescattering mode, and squares include the effect of parton fragmentations. The observed power law dependence of the net-baryon density as a function of Q_0 stems from the properties of the pQCD cross sections in the PCM. The absence of a saturation at small values of Q_0 indicates that not all valence quarks are "liberated" in the range of cutoff values considered here. Indeed, we find that the liberation factor for quarks in the nuclear parton distributions varies from about 0.7 for $x > 0.1$ to about 0.2 for $x \approx 0.01$. Figure 3 can be used to rescale the PCM prediction for the net-baryon rapidity distribution in Fig. 2 to other values of

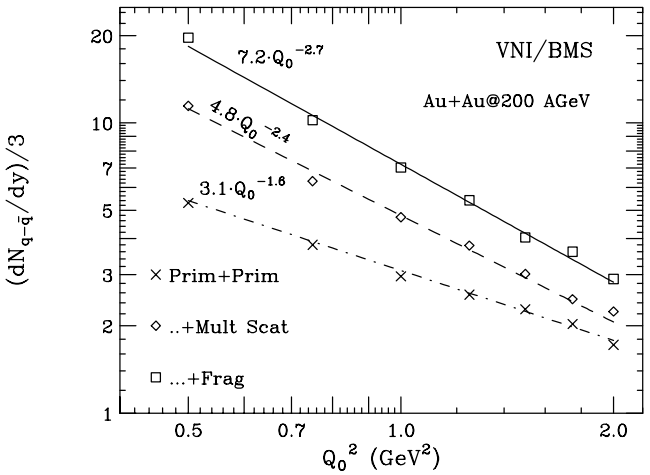

FIG. 3. Initialization scale and cutoff dependence of the net baryon density at midrapidity for Au + Au collisions at $\sqrt{s_{NN}} = 200$ GeV.

Q_0. For the range of Q_0 values extracted from RHIC data the PCM is well able to describe the measured net-baryon excess.

This success raises the obvious question: what does our model predict for the net-baryon distribution at lower energies? We have reported [24] recently that the partonic cascades provide only a dilute medium at SPS energies ($\sqrt{s_{NN}} \approx 20$ GeV), which does not support enough multiple scattering among partons to justify a perturbative treatment. This implies that partonic cascades having $p_T > p_T^{\min}$ constitute only a small part of the dynamics of the collision at SPS energies. Indeed we find that the net-baryon multiplicity at central rapidity in Pb + Pb collision at $\sqrt{s_{NN}} = 17.4$ GeV is only about 20% of the experimental value estimated by the NA49 experiment [25]. Similar considerations also apply to $p + p$ collisions, which do not produce a dense partonic medium where color screening occurs at a perturbative scale $p_T^{\min} > \Lambda_{\mathrm{QCD}}$. The transport of net-baryon number then must be due to nonperturbative mechanisms. The situation is dramatically different in Au + Au collisions at RHIC energies, where multiple parton scattering at $p_T > p_T^{\min}$ produces a medium, in which color is screened at a sufficiently short distance to allow for a choice of $p_T^{\min}$ in the domain of pQCD.

In conclusion, we find that the parton cascade model predicts a net-baryon excess at midrapidity in Au + Au collisions at RHIC, which is in qualitative agreement with the measured values. Two mechanisms are driving this excess: One is the presence of a net-baryon density in the initial state parton distributions at Bjorken-x around 0.01 reflecting the size of the valence quark component in this range of x. The other important factor is the rescattering among partons, which transports more partons, and hence additional net-baryon number, to midrapidity. This transport mechanism increases the net-baryon number density well into the range of measured values.

This work was supported in part by RIKEN, the Brookhaven National Laboratory, DOE Grants No. DE-FG02-96ER40945 and No. DE-AC02-98CH10886, and by the Natural Sciences and Engineering Research Council of Canada.

[1] STAR Collaboration, C. Adler *et al.*, Phys. Rev. Lett. **87**, 262302 (2001); (E) (to be published); PHENIX Collaboration, K. Adcox *et al.*, Phys. Rev. Lett. **89**, 092302 (2002).
[2] Itzhak Tserruya (private communication).
[3] BRAHMS Collaboration, P. Christiansen *et al.*, nucl-ex/0212002.
[4] S. A. Bass *et al.*, Nucl. Phys. **A661**, 205 (1999).
[5] L. D. McLerran and R. Venugopalan, Phys. Rev. D **49**, 3352 (1994); E. Iancu and L. D. McLerran, Phys. Lett. B **510**, 145 (2001); L. McLerran, Nucl. Phys. **A699**, 73 (2002).
[6] J. Schwinger, Phys. Rev. **82**, 664 (1951); N. Glendenning and T. Matsui, Phys. Rev. D **28**, 2890 (1983); H. Sorge, A. v. Keitz, R. Mattiello, H. Stöcker, and W. Greiner, Phys. Lett. B **243**, 7 (1990); A. v. Keitz, L. Winckelmann, A. Jahns, H. Sorge, H. Stöcker, and W. Greiner, Phys. Lett. B **263**, 353 (1991); F. Cooper, J. M. Eisenberg, Y. Kluger, E. Mottola, and B. Svetitsky, Phys. Rev. D **48**, 190 (1993); T. Schönfeld, H. Stöcker, W. Greiner, and H. Sorge, Mod. Phys. Lett. A **8**, 2631 (1993); Z.W. Lin, S. Pal, C. M. Ko, B. A. Li, and B. Zhang, Phys. Rev. C **64**, 011902 (2001).
[7] D. Kharzeev, Phys. Lett. B **378**, 238 (1996); A. Capella and B. Z. Kopeliovich, Phys. Lett. B **381**, 325 (1996).
[8] S. E. Vance, M. Gyulassy, and X. N. Wang, Phys. Lett. B **443**, 45 (1998); S. E. Vance and M. Gyulassy, Phys. Rev. Lett. **83**, 1735 (1999).
[9] G. C. Rossi and G. Veneziano, Nucl. Phys. **B123**, 507 (1977); L. Montanet, G. C. Rossi, and G. Veneziano, Phys. Rep. **63**, 149 (1980); B. Z. Kopeliovich and B. G. Zakharov, Sov. J. Nucl. Phys. **48**, 136 (1988); Z. Phys. C **43**, 241 (1989); Phys. Lett. B **211**, 221 (1988); E. Gotsman and S. Nusinov, Phys. Rev. D **22**, 624 (1980).
[10] M. Glück, E. Reya, and A. Vogt, Z. Phys. C **67**, 433 (1995).
[11] W. Busza and A. S. Goldhaber, Phys. Lett. B **139**, 235 (1984); W. Busza and R. Ledoux, Annu. Rev. Nucl. Part. Sci. **38**, 119 (1988).
[12] K. Geiger and B. Müller, Nucl. Phys. **B369**, 600 (1992).
[13] K. Geiger, Phys. Rep. **258**, 237 (1995); Comput. Phys. Commun. **104**, 70 (1997).
[14] S. A. Bass, B. Müller, and D. K. Srivastava, Phys. Lett. B **551**, 277 (2003).
[15] E. V. Shuryak and M. A. Stephanov, Phys. Rev. C **63**, 064903 (2001).
[16] R. Cutler and D.W. Sivers, Phys. Rev. D **17**, 196 (1978); B. L. Combridge, J. Kripfganz, and J. Ranft, Phys. Lett. B **70**, 234 (1977).
[17] M. Bengtsson and T. Sjöstrand, Phys. Lett. B **185**, 435 (1987); Nucl. Phys. **B289**, 810 (1987).
[18] L. V. Gribov, E. M. Levin, and M. G. Ryskin, Phys. Rep. **100**, 1 (1983); D. Kharzeev and M. Nardi, Phys. Lett. B **507**, 121 (2001); D. Kharzeev, E. Levin, and M. Nardi, hep-ph/0111315.
[19] T. Sjostrand and M. van Zijl, Phys. Rev. D **36**, 2019 (1987).
[20] N. Abou-El-Naga, K. Geiger, and B. Müller, J. Phys. G **18**, 797 (1992).
[21] K. J. Eskola and H. Honkanen, Nucl. Phys. **A713**, 167 (2003).
[22] K. J. Eskola, K. Kajantie, P. V. Ruuskanen, and K. Tuominen, Nucl. Phys. **B570**, 379 (2000).
[23] A. Krasnitz, Y. Nara, and R. Venugopalan, Nucl. Phys. **A717**, 268 (2003).
[24] S. A. Bass, B. Muller, and D. K. Srivastava, Phys. Rev. C **66**, 061902 (2002).
[25] NA49 Collaboration, H. Appelshauser *et al.*, Phys. Rev. Lett. **82**, 2471 (1999).